JOURNAL OF GEOPHYSICAL RESEARCH, VOL. 96, NO. A7, PAGES 11,271–11,282, JULY 1, 1991

ULF WAVES UPSTREAM OF THE VENUS BOW SHOCK: PROPERTIES OF ONE-HERTZ WAVES

D. S. Orlowski and C. T. Russell

Institute of Geophysics and Planetary Physics, University of California, Los Angeles

Abstract. Pioneer Venus orbiter data are used to examine the properties of a class of ULF upstream waves with relatively high observed frequencies (1.1 - 1.3 Hz). In the spacecraft frame these waves are most often left-hand elliptically polarized. They have amplitudes up to 3 nT (near the bow shock) and propagate obliquely to the magnetic field at angles from 10° to 50°. These waves show significant similarity in their properties to "one-Hertz" waves identified at the Earth in the ISEE 1 and 2 observations and the whistler waves identified earlier with IMP 6 observations. The waves appear almost immediately after the spacecraft crosses the magnetic field tangent line to the bow shock surface into the region of connected field lines. The amplitude of these waves decreases with distance from the shock measured along the magnetic field line. We have used the cold plasma dispersion relation in order to study the propagation of these waves and to explain their observed polarization. Calculated group velocities indicate that those waves have sufficient upstream velocities to propagate from the shock into the solar wind. The totality of observations, including the observed wave damping and the observation of right-handed waves, seems best explained by a source of right-handed whistler mode waves at the bow shock.

Introduction

The region upstream of the Earth's bow shock has been extensively studied and analyzed for more than two decades. For reviews and original works, see Fairfield [1969, 1974], Gary [1981], Greenstadt et al. [1968, 1981], Gurnett [1985], Hoppe and Russell [1980], Hoppe et al. [1981, 1982], Russell et al. [1971], Russell and Hoppe [1983], and Russell [1985]. These early studies showed that the physical phenomena occurring at the bow shock were governed by its local surface geometry, parameterized by the angle between the normal to the model shock surface and the direction of the interplanetary magnetic field (IMF), θ_{Bn}. From plasma kinetic theory, together with high temporal and angular resolution measurements, we now understand that microphysical processes such as the reflection and acceleration of electrons and ions at the shock are important [Sonnerup, 1969; Gary, 1981; Sentman et al., 1981]. These reflected and accelerated particles can stream back along magnetic field lines and cause a variety of instabilities and attendant waves. Many of these phenomena have been studied in front of the Earth's bow shock. However, it is useful to examine some of these phenomena at a different planet for several reasons. First, the solar wind properties vary with heliocentric distance. This variation may induce some change in these phenomena that will provide useful diagnostics concerning the underlying instability. Second, a planet like Venus has a more stable shock position than Earth because the shock location does not depend on the dynamic pressure of the solar wind. Thus, geometrical studies may be more easily performed there. Third, the radius of curvature of the Venus bow shock is significantly smaller than that of the terrestrial bow shock. This may affect reflection and/or acceleration of the particles by the shock. It is the purpose of this paper to exploit the Pioneer Venus Orbiter data to examine in detail one of the upstream wave phenomena that have been reported at Venus.

The waves in the solar wind on magnetic field lines connected to the Venus (and terrestrial) foreshock can be divided into two classes according to their frequency. The first class consists of intense waves with $f_o/f_{gi} < 1$ where f_o is the observed frequency and f_{gi} is the proton gyrofrequency. The second class consists of weak waves with $f_o/f_{gi} > 1$ which have been found at Mercury, Venus, and the Earth [Orlowski et al., 1990]. We focus our analysis here on the second class, leaving low-frequency upstream waves for future investigation. Herein, we give a detailed analysis and description of these relatively high frequency electromagnetic waves observed at Venus together with estimates of their properties such as ellipticity, polarization, and propagation vector derived from the imaginary part of the power spectral matrix using the method developed by Means [1972]. We also examine the location of the observed waves relative to the expected geometry of the electron foreshock of Venus, discuss the mode of propagation of these waves, and examine possible mechanisms.

Instrumentation and Data

For our study we have used magnetic field data from University of California, Los Angeles, flux gate triaxial magnetometer on the Pioneer Venus orbiter (PVO) with a dynamic range of 128 nT and a precision of 1/16 nT [Russell et al., 1980]. Due to the relatively high upper limit of the frequencies of interest we selected only data with high time resolution (≥ 4 s^{-1}). For our most detailed analysis (power spectra and tables) we used data at only the very highest temporal resolution (12 vectors s^{-1}). These latter data are available only near inferior conjunction and only for a limited amount of time each orbit. In order to examine the expected propagation and Doppler shifting of these waves we will use solar wind measurements returned by the PVO plasma analyzer [Intriligator et al., 1980].

Observations

High-resolution magnetic field data were examined for 30 orbits selected from orbits 551 to

Paper number 91JA01103.
0148-0227/91/91JA-01103$05.00

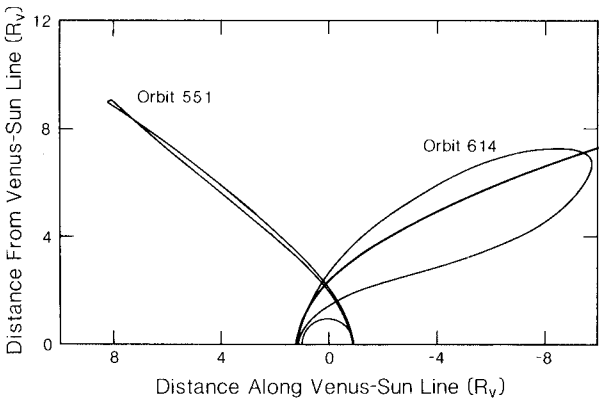

Fig. 1. Typical orbits of the Pioneer Venus orbiter characteristic of the period studied, plotted in solar cylindrical coordinates. The average shape of the Venus bow shock is also shown.

614, which covered the period from June 8, 1980, to August 11, 1980. Two typical orbits of this sequence are shown in Figure 1. The low-frequency waves $f_o/f_{gi} < 1$ were found to be a commonly observed feature in the data of each of the 30 orbits. In the data from 16 of these orbits we found waves with $f_o/f_{gi} > 1$. A good example of these waves is shown in Figure 2, where the three magnetic field components and the magnitude are plotted versus time. The B_x, B_y, B_z components of the magnetic field vector are displayed in Venus Solar Orbital (VSO) coordinates in which the x axis points toward the Sun, the z axis points along the Venus orbital pole, and the y axis points opposite to the planetary motion. The waves are seen clearly in the absence of any low-frequency component, and the magnetic field strength is almost constant. The results of spectral analysis are shown in the right-hand panel of Figure 2. There is a very distinct peak with the intensity about 0.7 nT^2/Hz and frequency about 1.4 Hz. Wave analysis using both the principal axis method [Born and Wolf, 1959] and the Means method [Means, 1972] indicates that the waves are left-hand elliptically polarized in the spacecraft frame with an ellipticity of about 0.97 and that they propagate obliquely at an angle θ_{kB} of 36° to the magnetic field. The wave normal points within about 20° of the solar wind flow direction, θ_{Bx}. Another important feature in these spectra is the strong decrease of the wave power with increasing frequency (about 160 dB/decade) at frequencies between approximately 1.5 Hz and the Nyquist frequency. This cutoff is much sharper than the falloff of the antialiasing filter in the instrument and occurs well below that frequency. The waves shown in Figure 2 were observed at a distance of 3.5 R_V from the shock. However, not all waves observed during selected periods are left-handed. For example,on July 3, 1980,between 1426 and 1430 UT,right-hand polarized waves were observed during the outbound leg of the orbit. These waves have similar amplitudes, ellipticities, propagation angles, and frequency range to the left-handed waves. In contrast to the left-handed waves, these waves propagate at a large angle, 64°, to the solar wind velocity and were observed on this day only at distances less than 1 R_V from the bow shock. An example of these right-handed waves is given in Figure 3.

Results of the detailed wave analysis for six intervals of the wave observations from orbits 571, 572, 576, 580, 581, and 585, from time intervals ranging from 3 to 32 min, are shown in Table 1. This table contains the date and the time interval for each of the six reported events, the observed frequency in the spacecraft frame in Hertz, the amplitude of the wave (in nanoTeslas) derived from the trace of the power spectral matrix, the polarization, the ellipticity as a ratio between the longer and shorter axis of the propagation ellipse, the unit vector parallel to the propagation direction derived from the antisymmetric component of the power spectral matrix using the method by Means [1972], and the unit vector parallel to the averaged magnetic field direction. We include in Table 1 the angle between the propagation vector and the x axis, θ_{kx}; the angle between k and the IMF direction, θ_{kB}; and the angle between the IMF direction and the shock

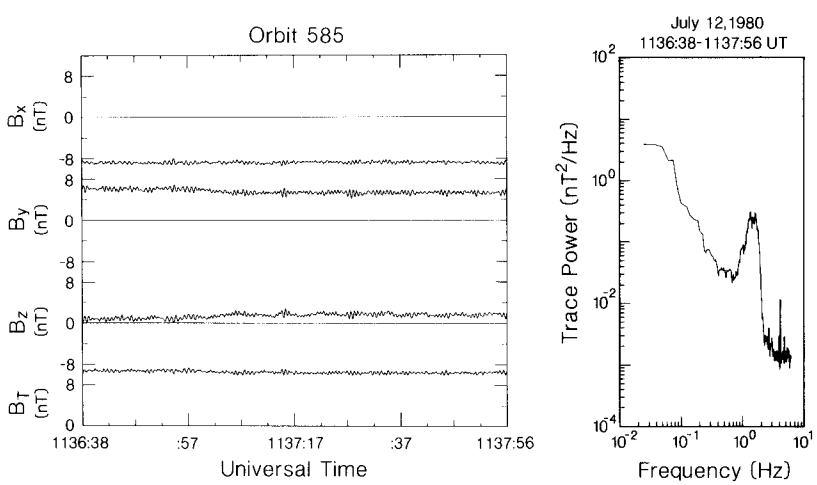

Fig. 2. High-resolution time series of three components of the magnetic field and its magnitude showing wave trains and packets at approximately 3.5 R_V upstream of the Venus bow shock. (Right) Power spectra of the magnetic fluctuations exhibiting a very distinct peak at about 1.4 Hz.

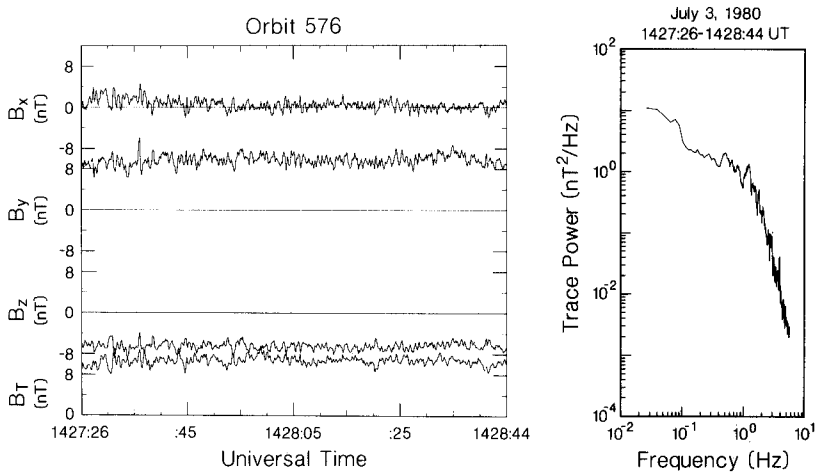

Fig. 3. An example of the time series and power spectra of the right-hand elliptically polarized wave recorded on July 3, 1980.

normal, θ_{Bn}, at the point where the IMF field line through the spacecraft intersects the shock. We find that these waves are generally left-hand elliptically polarized in the spacecraft rest frame as illustrated in the hodogram in Figure 4. They are typically observed in the frequency range from 0.7 to 1.3 Hz propagating obliquely to the magnetic field at an average angle θ_{kB} less than 40°.

Figure 5 shows the measured angle of propagation for 97 analysis intervals taken from the 30 orbits examined. The waves are clearly strongly guided by the magnetic field. The histogram peaks from 20° to 30°. Only 2% of the wave events propagate at angles of greater than 40° to the magnetic field, and none greater than 60°. These statistics are very reminiscent of the results of Fairfield's [1974] study of whistler waves upstream from the Earth's bow shock. Their Figure 7, which includes 84 wave events, shows a peak from 30° to 40° with 6% at angles greater than 60°.

Figure 6 illustrates the range of angles found between the wave vector and the solar direction, θ_{kx}. It also illustrates another curious fact. The frequency of the waves and their polarization are controlled by this angle. Waves which are most nearly propagating along the flow direction are left-handed and at largest frequencies. As the wave vector becomes more nearly perpendicular to the flow, the frequency drops slightly, and then suddenly the polarization reverses and the wave becomes right-handed. The switchover is at about 47°. Again a similar result was obtained for the Earth by Fairfield [1974], who found a majority of waves to be right-hand polarized in contrast to our left-handed majority. At Earth as illustrated in his Figure 8, the wave frequency increases from low left-hand polarized values to high right-hand values crossing from left to right polarization at about 40°.

Since the waves are strongly guided by the magnetic field, we would expect that the angle with the field and the angle of propagation with the flow would be highly correlated. Thus as the angle θ_{Bx} varied from parallel to perpendicular, the polarization would again be expected to change from left to right. Figure 7 shows that is indeed the case with a polarization switch at about 75°. Again this compares favorably with the polarization switch found by Fairfield (his Figure 6) at about 60°.

The wave amplitudes observed range from about 0.3 to 3 nT (δ B/B = 0.06 to 0.13). Part of the variability in amplitude appears to be the distance from the shock. Figure 8 shows the measured wave amplitudes with a bandwidth of 1 Hz centered at 1.3 Hz for our 97 analysis intervals as a function of the distance from the shock to the spacecraft along the interplanetary magnetic

TABLE 1. Characteristics of Observed Wave Events

Date Time	Frequency,Hz	Amplitude,nT	Polarization	Ellipticity	k,VSO	b,VSO	θ_{kB}	θ_{Bn}	θ_{kx}
June 28, 1358-1407	1.1	1.15	L	1.08	(0.98,-0.05,-0.18)	(0.86,-0.36,-0.04)	20°	57°	11°
June 29, 1044-1108	1.1	0.71	L	1.04	(0.89,-0.25,-0.36)	(0.72,-0.68,-0.03)	28°	28°	27°
July 3, 1426-1430	1.3	0.79	R	1.06	(0.44,0.33,-0.83)	(0.01,0.72,-0.68)	34°	69°	64°
July 7, 1445-1455	1.3	1.10	L	1.10	(0.97,-0.12,-0.15)	(0.78,-0.44,-0.11)	25°	49°	14°
July 8 1457-1500	1.3	0.98	L	1.04	(0.99,-0.39,0.01)	(0.71,0.24,-0.54)	43°	37°	8°
July 12, 1135-1208	1.3	0.75	L	1.06	(0.87,-0.42,0.21)	(-0.79,0.59,0.02)	19°	32°	30°

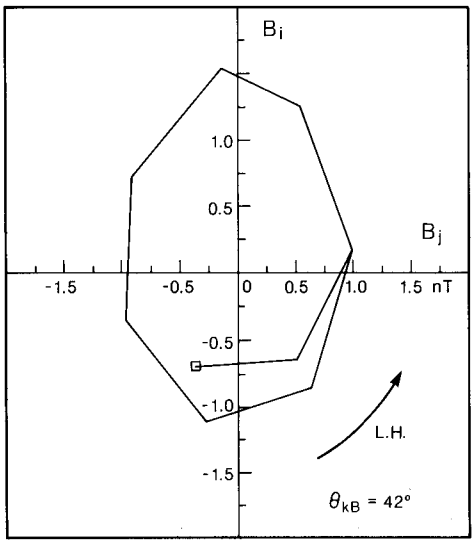

Fig. 4. An example of a hodogram of the wave component contained in the principal plane as measured on orbit 585 on July 12, 1980. Significant ellipticity and a left-handed sense of rotation relative to the magnetic field are observed. The magnetic field is pointing into the plane of the page.

field line. The average amplitude of the waves decreases with a scale length of 10 R_V. No obvious difference in amplitude was seen for left-handed and right-handed waves, and both polarizations were found independent of distance from the shock. The variation in amplitude at fixed distance from the bow shock may be due to different strength sources above different points on the shock. This strength may be controlled by the local Mach number and θ_{Bn} of the shock and hence dependent on the shock geometry. We discuss the shock geometry further in a later section.

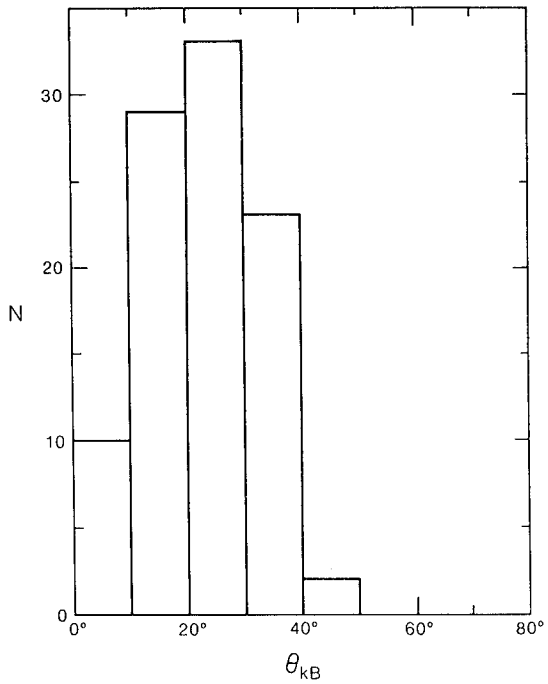

Fig. 5. Histogram of the number of times the angle between the wave normal vector and the magnetic field, θ_{kB}, lay at differing angles. Ten-degree bins were used.

Comparison With Cold Plasma Dispersion Relation

Studies by Russell et al. [1971], Holzer et al. [1972], Fairfield [1974], and Hoppe et al. [1981, 1982] show waves at Earth with properties similar to those reported above. These authors all found a class of waves at approximately 1 Hz propagating upstream of the Earth bow shock with average angle

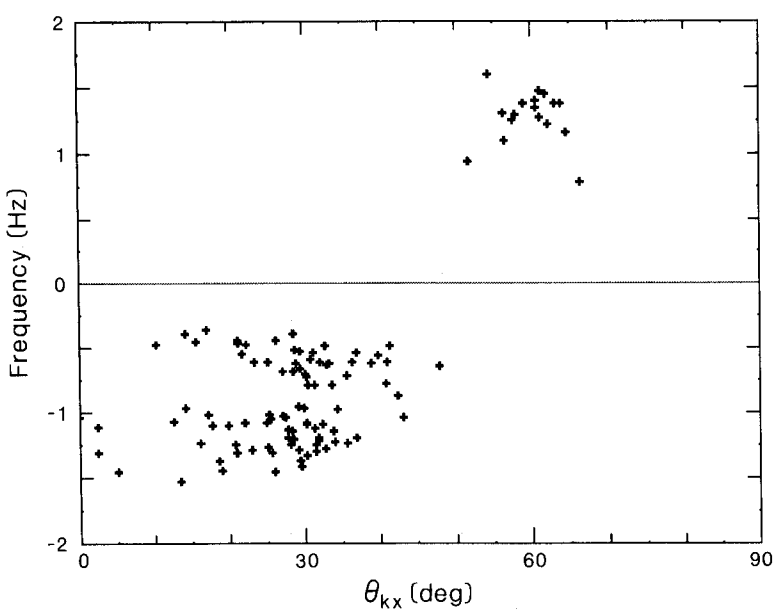

Fig. 6. The frequency of the "1-Hz" waves as a function of their direction of propagation relative to the solar direction. Negative frequencies are left-handed relative to the magnetic field in the spacecraft frame.

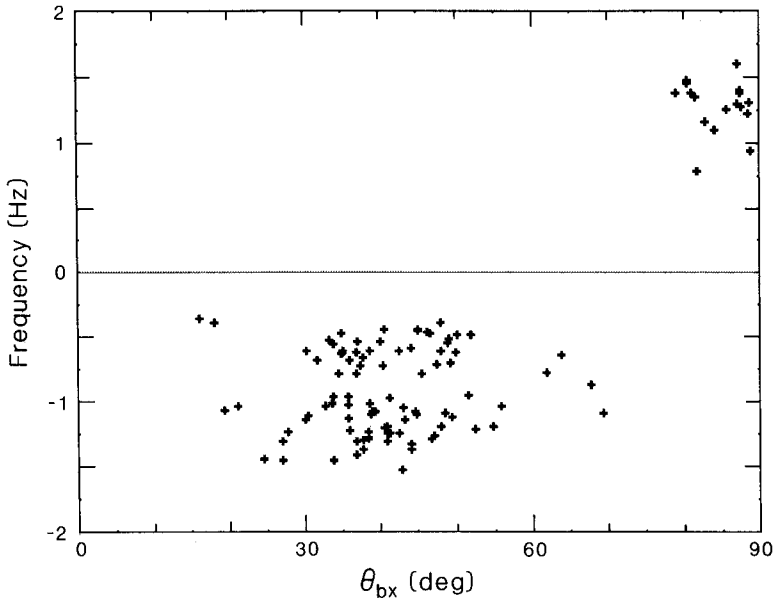

Fig. 7. The frequency of the 1-Hz waves as a function of the magnetic field relative to the solar direction. Negative frequencies are left-handed in the spacecraft frame.

to the IMF of 45°. Fairfield [1974] showed that these waves could be explained in terms of whistler mode waves propagating upstream from the shock. Using simultaneous measurements from ISEE 1 and 2, Hoppe et al. [1982] confirmed the propagation mode of those waves to be the whistler mode by measuring the wavelength and direction of propagation and by comparing the predictions of the cold plasma dispersion relation (CPDR), using the measured solar wind properties and magnetic field. The study by Hoppe et al. [1982] suggests that the dispersion of these waves is relatively well described by the cold plasma approximation. We expect the CPDR to be accurate for whistler waves where the phase velocity, V_{ph}, is much greater than the sound speed, C_s, and the Alfven speed, V_A, and at frequencies relatively far from the resonant ones. We have also applied the CPDR to study the propagation of our waves to explain their observed polarization assuming that the waves propagate against the solar wind flow as do those at Earth's foreshock. We used the general dispersion relation for the "cold" plasma approximation after Stix [1962]. The observed frequency of the wave propagating upstream, in the presence of Doppler shifts caused by the solar

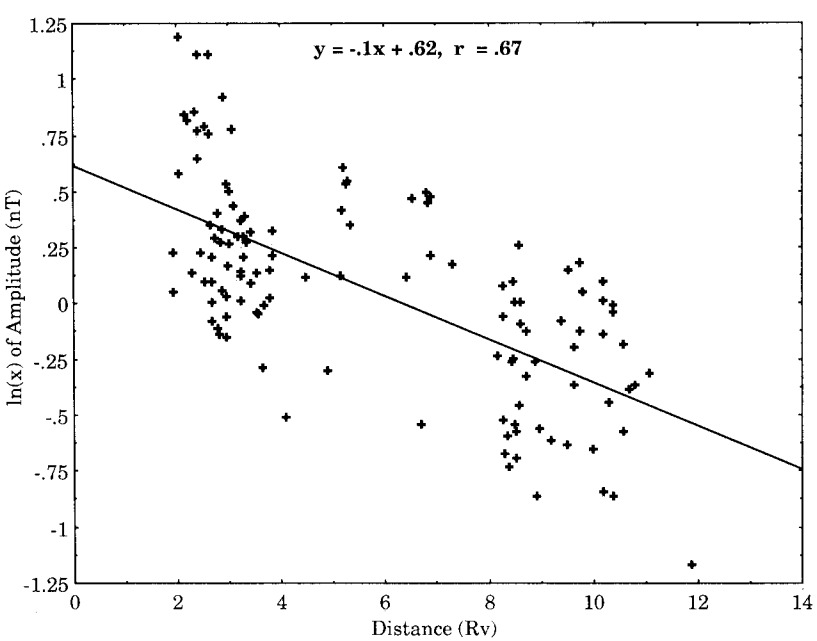

Fig. 8. The amplitude of the waves in the frequency range from 0.8 Hz to 1.8 Hz versus distance from the shock as measured along the interplanetary magnetic field.

wind flow relative to the spacecraft, can be expressed by

$$\omega_o = \omega_i - kV_{sw}\cos(\theta_{kx}) \quad (1)$$

where

k wave number;
$\omega_o/2\pi$ wave frequency in the spacecraft frame;
$\omega_i/2\pi$ wave frequency in the plasma frame;
V_{sw} solar wind velocity;
θ_{kx} angle between k vector and solar wind flow.

We have solved numerically both the CPDR and (1), using measured solar wind data and averaged IMF contained in Table 2. An example of the dispersion relation calculated for the waves measured on July 12, 1980, is shown in Figures 9a and 6. The results are summarized in Tables 3 and 4.

Examination of Table 3 indicates that our solutions should be in the range where the cold plasma approximation is correct within the accuracies of our measurements. This is to be expected since the obtained phase velocities are all about 6 times greater than V_A and C_s, which range from 40 km/s to 55 km/s. Most waves observed to be left-handed (if the k vector points toward the Sun) will be in fact right-hand polarized in the plasma frame because their phase velocity is always less (by 50 to 70 km/s) than the solar wind velocity projected on the k vector. Only in the case of the observed right-handed waves is the phase velocity (67 km/s) greater than the V_{sw} component parallel to the k vector, so that the phase fronts can propagate upstream against the solar wind. The plasma rest frame frequency of the waves ranges typically from 19 to 62 times proton gyrofrequency. The wavelengths range from 30 to 58 km, which indicates a relatively small spread in the wave vector magnitude. All the above results are consistent with those at the Earth reported by Fairfield [1974], Hoppe and Russell [1980], and Hoppe et al. [1981, 1982].

Location of Observed Waves Relative to Venus Bow Shock

To locate our measurements with respect to the plasma boundaries we use a model of the foreshock geometry [Crawford et al., 1990]. We need such a model because the foreshock waves are position dependent. Such a coordinate system was first proposed by Greenstadt and Baum [1986] for Earth and by Greenstadt et al. [1987] for Venus. This approach enables us to represent the spacecraft position relative to the bow shock in two

TABLE 2. Solar Wind Properties at Venus

Date, 1980	Solar Wind Density, cm^{-3}	Solar Wind Velocity, km/s	IMF nT
June 28	19	302	8.6
June 29	25	310	10.0
July 03	32.5	338	13.4
July 07	12	461	8.6
July 08	15.2	435	10.3
July 12	22	395	11.0

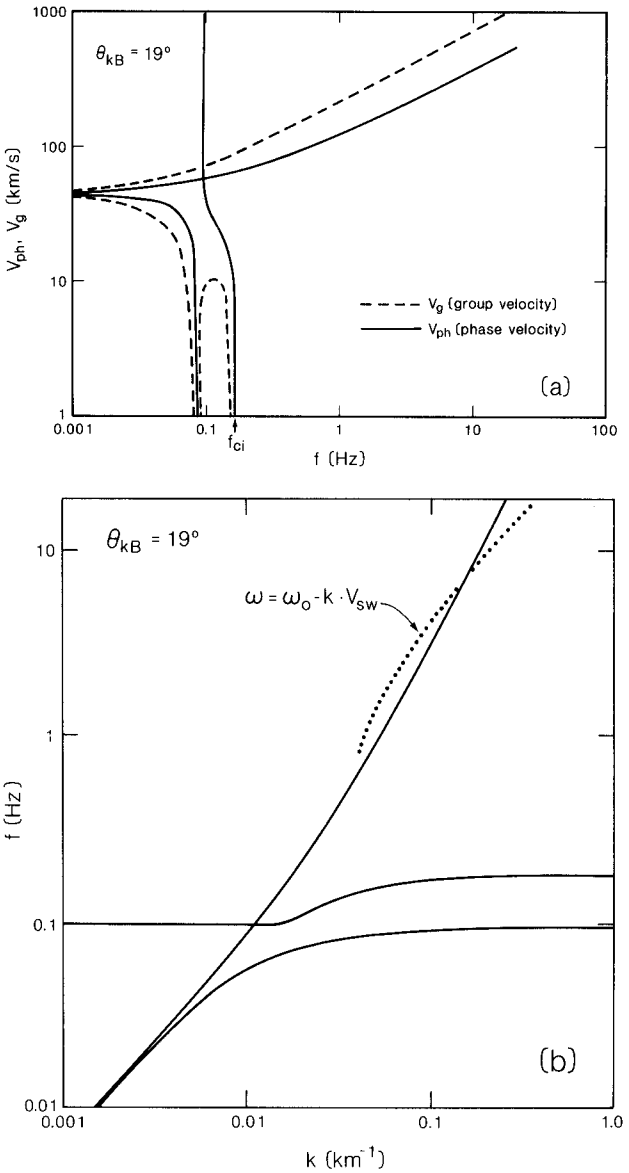

Fig. 9. An example of the cold plasma dispersion relation used for the calculation of wavelengths and phase and group velocities of the oblique waves. In this example, θ_{kB} is 19° as observed on July 12, 1980, when V_{sw} was 395 km/s, n was 22 cm^{-3}, and the average total B was 11 nT. (a) Phase velocity and group velocity versus frequency. (b) Frequency versus wave number.

dimensions, in the plane formed by V_{sw} and the IMF containing the intersection point of the bow shock and magnetic field line through the spacecraft. We express the spacecraft position relative to the IMF tangent line to the shock by FDepth and FDist as explained by Crawford et al., [1990]. FDepth is the distance behind the tangent line along the planet-Sun line, and FDist is the distance along the tangent line boundary from its intersection with the bow shock. We have divided our wave data into two groups. The first group contains wave data measured when the relative position of the spacecraft and the IMF tangent line characterized by FDepth is less than 5 R_V. The second group

TABLE 3. Frequencies of the One-Hertz Waves

Date, 1980	f_{ci}, Hz	f_p/f_{gi}	f_{lh}, Hz	f_p/f_{lh}	k, km^{-1}
June 28	0.13	36 ± 10	5.6	0.85 ± 0.25	0.12 ± 0.02
June 29	0.15	34 ± 6	6.5	0.78 ± 0.19	0.14 ± 0.02
July 3	0.20	21 ± 2	8.7	0.50 ± 0.06	0.13 ± 0.01
July 7	0.13	64 ± 10	5.6	1.48 ± 0.22	0.13 ± 0.01
July 8	0.16	69 ± 25	6.7	1.60 ± 0.60	0.17 ± 0.05
July 12	0.17	34 + 8	7.2	0.80 + 0.17	0.12 + 0.01

Notes: f_{gi} is proton gyrofrequency; f_p is wave frequency; f_{lh} is lower hybrid resonance frequency; and k is wave number.

covers cases when FDepth considerably exceeds that arbitrary limit. A good example of the wave data when FDepth is less than 5 R_V is shown in Figure 10. The spacecraft position relative to the modeled foreshock and wave spectra are presented in Figure 10a and 10c, respectively. In this case FDist is equal to approximately 9 R_V. Here there are no low-frequency waves while the higher-frequency component is very well distinguished in the spectrum. In this case, θ_{Bn} is about 50°. When FDepth is substantially greater than 5 R_V (on average), the picture of the observed waves may change. The dominant low-frequency turbulent component of the spectrum may appear with a well-distinguished higher- frequency wave in the form of trains and/or shocklets. An example of waves observed in the upstream region is shown in Figure 11. Figure 11a shows the spacecraft position relative to the shock, and Figure 11c contains spectra of the magnetic field fluctuations taken from the time period shown in Figure 11b. The application of the foreshock coordinates organizes the wave data both here and in all other intervals studied extremely well, showing that the foreshock geometry and the morphology of the upstream wave phenomena are related.

Such easy and simple parameterization of the magnetic foreshock region using only two planar coordinates is most accurate when the magnetic field direction changes slowly as the spacecraft moves through the region. Otherwise, we cannot define a stationary foreshock region in the bow shock frame. Moreover, this approach has certain limitations concerning the angle between the IMF direction and to the solar wind flow. If that angle, θ_{Bx}, is equal to or less than the model shock cone angle, the whole upstream region is connected to the shock regardless of the distance and location in the shock frame. In that case, no IMF tangent line to the shock can be defined, and therefore the coordinates cannot be calculated.

TABLE 4. Velocity of One Hertz Waves

Date, 1980	$\theta_{Bx,deg}$	$\theta_{gx,deg}$	V_{gx}/V_{sw}	V_{ph}/V_{swx}
June 28	30.7	9.5	1.30 ± 0.18	0.81
June 29	43.9	12.9	1.00 ± 0.12	0.82
July 3	89.4	15.3	0.01 ± 0.01	1.91
July 7	38.7	11.4	1.29 ± 0.15	0.86
July 8	44.8	16.9	1.25 ± 0.16	0.89
July 12	37.8	9.1	1.07 + 0.13	0.81

Notes: θ_{gx} is the angle between wave group velocity and magnetic field; θ_{Bx} is the angle between the magnetic field and the solar direction; V_{gx} is the wave group velocity derived from the cold plasma dispersion relation, projected on the flow direction; V_{ph} is the wave phase velocity from the cold plasma dispersion relation; and V_{swx} is the component of the solar wind velocity in the antisolar direction along the k vector.

Transition Between a Quasi-Parallel and a Quasi-Perpendicular Configuration

An example of wave observations during the transition between a quasi-parallel and quasi-perpendicular shock geometry seen from about 1 R_V from the shock is found on July 7, 1980 between 1452:00 - 1453:30 UT. In Figure 12 θ_{Bn} measured at the intersection point of the three-dimensional shock and the IMF through the spacecraft versus time. As seen from Figure 12, there is a sharp increase in θ_{Bn} at 1453:22 from 42° (spacecraft connected to the quasi-parallel shock) to about 65° (spacecraft connected to the quasi-perpendicular bow shock) in less than 2 min. The crossing of the formal division line between quasi-parallel and quasi-perpendicular shock geometry is remarkably well correlated with the apparent change of the character of the magnetic field fluctuations, i.e., from turbulent, low-frequency dominated (characteristic of the ion foreshock) to quiet and strictly confined to a narrow frequency band (characteristic of the electron foreshock). Two consecutive spectra (Figure 13), taken when θ_{Bn} is greater and less than the nominal 45°, confirm the significant decrease of the wave intensity at lower frequencies between about 0.05 and about 1 Hz.

Crossing of the Tangent Field Line

The waves studied by Fairfield [1974] were principally observed within a few minutes of the bow shock with a few events observed several hours from the bow shock. Fairfield [1974] naturally associated these waves with the bow shock as did Holzer et al. [1972]. The wave events studied by Hoppe et al. [1982] (see their Table 1) ranged from 1 to 8 R_E from the bow shock and were thought to be different than the waves studied by Fairfield [1974].

Initially, these distant 1 Hz waves at the Earth were believed to be associated with the upstream ions [Hoppe et al., 1981, 1982], but no clear and consistent association with any ion beam property was found. Feldman et al. [1983] showed an association between 1 Hz waves and

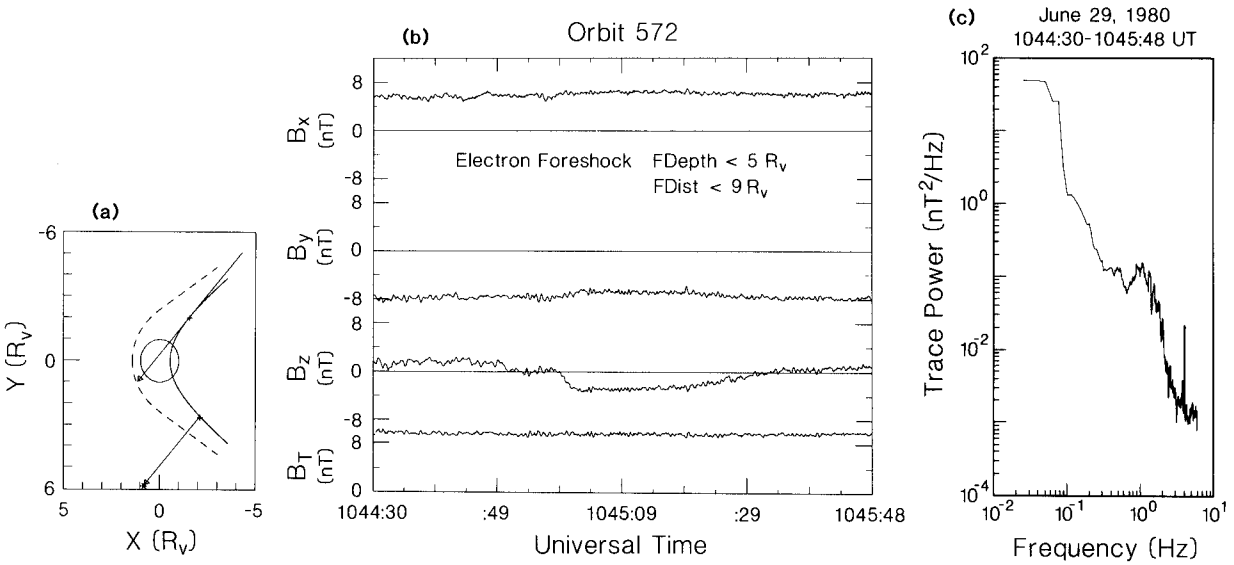

Fig. 10. An example of the magnetic field data measured by the magnetometer at about 5 R_V from the quasi-parallel shock. (a) The spacecraft position, indicated by a cross, relative to the shock tangent line in the plane formed by B and V_{sw}. The dashed line is the shock front intersecting the B-V plane passing through the center of the plane. The solid line gives the shock front intersecting the B-V plane passing through the spacecraft. (b) Time series of the three components of the magnetic field and its magnitude measured at the position indicated in Figure 10a. (c) Power spectra obtained from time series shown in Figure 10b.

backstreaming electrons heated and accelerated at the bow shock. The appearance of those waves was highly correlated with the crossings of the IMF tangent line, the most solarward field line to intersect Earth's bow shock. Thus, if either Fairfield's [1974] interpretation is correct (propagation from shock) or Feldman et al.'s [1983] (generation in the electron foreshock), we might expect to see these waves arise shortly after connection of the IMF to the bow shock.

Data obtained at Venus on July 7, 1980, provide an example of the wave data as this connection occurs at the interface between field lines magnetically connected to the shock and those unconnected. In Figure 14 there is a sequence of two successive foreshock geometries as the spacecraft "moved" within a 15-s interval showing the disconnection of the field line from the

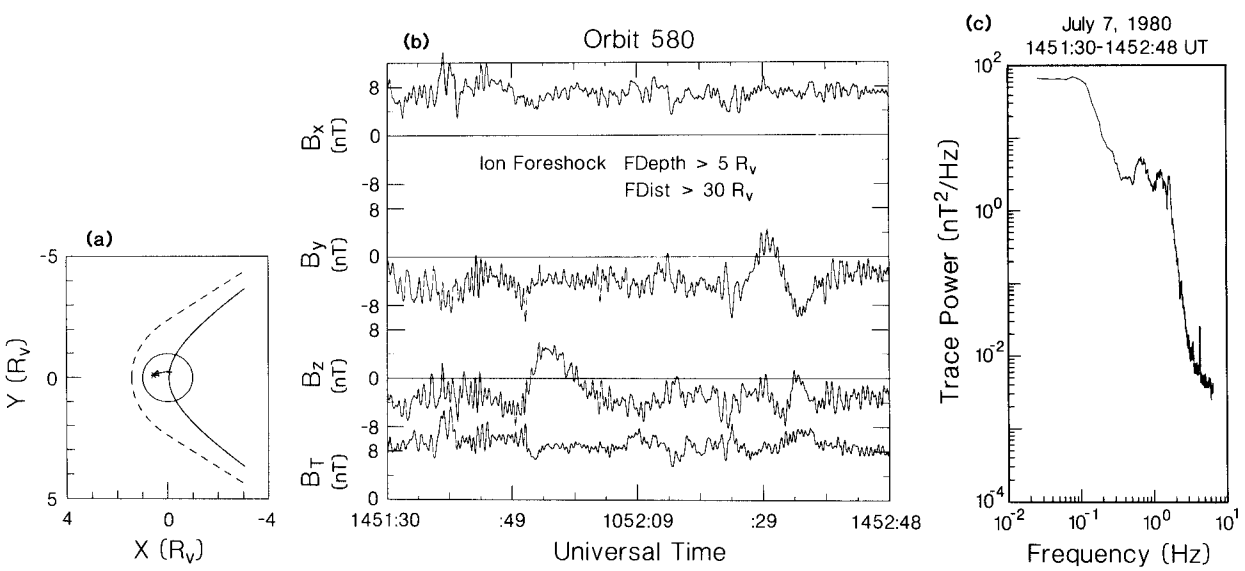

Fig. 11. An example of the magnetic field data measured by the magnetometer in front of the nose of the quasi-parallel shock (0.5 R_V). a) Spacecraft position indicated by a cross, relative to the shock in the plane formed by B and V_{sw}. b) Time series of the three components of the magnetic field and its magnitude measure at the position indicated in panel a). c) Power spectra obtained from time series shown in panel b) using the Fast Fourier Transform method with a frequency resolution about 0.12 Hz.

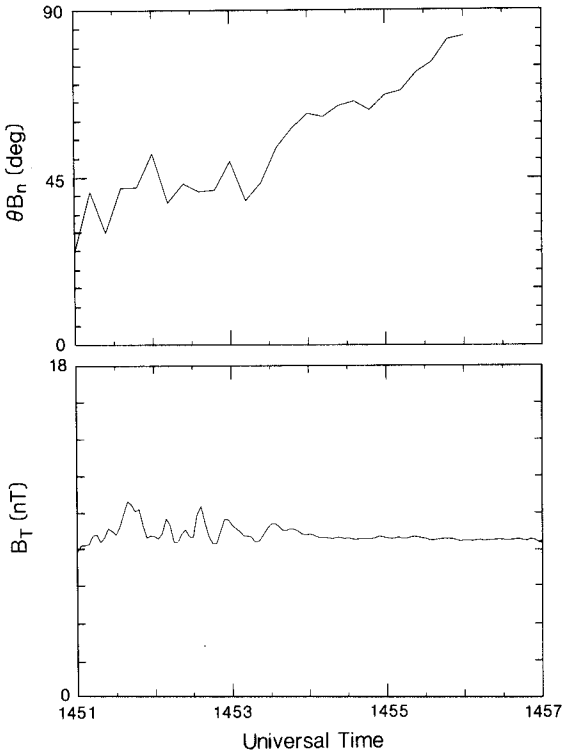

Fig. 12. Changes in the apparent character of the magnetic field fluctuations correlated with θ_{Bn}. (Top) θ_{Bn} versus time, showing nominal transition point from quasi-parallel to quasi-perpendicular shock observed less than 1 R_V upstream in the solar wind flow. (Bottom) Time series of the magnitude of the magnetic field from the same period of time. Apparent is the change in character of the magnetic fluctuations from ion foreshock-like to electron foreshock-like which is well correlated with the transition shown in the top panel.

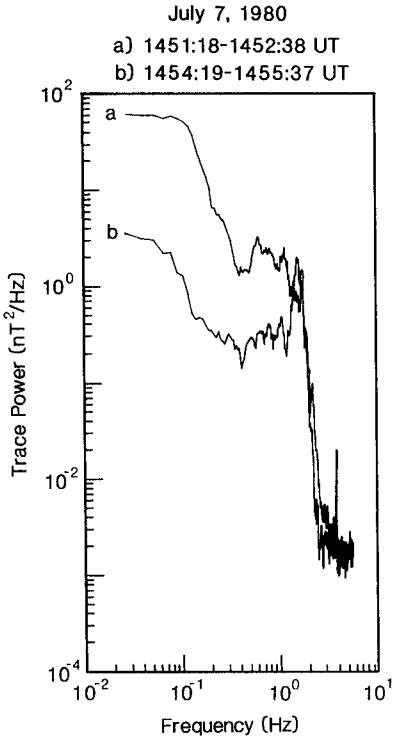

Fig. 13. Spectra of the magnetic field fluctuations calculated from the time series contained in Figure 9 showing a significant decrease of the wave emissions at frequencies less than approximately 1 Hz when the spacecraft moves to lines for which θ_{Bn} is greater than 45°.

shock. As shown in Figure 14, the modeled disconnection is very well correlated with the changing of the apparent character of the magnetic field fluctuations. This effect is clearly seen in the two consecutive spectra labeled "a" and "b" taken before and after the disconnection and shown in Figure 14d. The decrease of the high-frequency wave intensity by about 2 orders of magnitude is quite evident, indicating the absence of those waves in the unconnected solar wind. Thus, the high-frequency waves are controlled by connection to the foreshock.

Discussion

In this work we have studied relatively high frequency electromagnetic waves in the Venus foreshock typically at frequencies of 1.0-1.3 Hz. Although the majority of the waves have been observed to be left-hand polarized, a significant fraction of the waves are right-handed. We attribute the polarization reversal to be due to Doppler shifting of upstream propagating waves by the solar wind. We are not able to verify the sign of the direction of propagation unambiguously from the single-spacecraft measurements available at Venus. However, similar waves at Earth are found to be propagating in the upstream direction against the solar wind. Moreover, such an assumption is strongly supported by the fact that all the waves which are observed to be left-hand polarized propagate with a phase velocity less than the solar wind velocity projected on the direction of the wave vector while the wave front of the right-handed waves propagates faster than plasma flows along the k vector. Statistically we find that the polarization reversal occurs at a θ_{kB} angle of 75° and a θ_{Bx} of 47°. Further, assuming that the waves are whistler mode waves attempting to propagate upstream we are able to explain almost all the observed wave properties (including differences in polarizations). Use of the cold plasma dispersion relation shows that all the waves which are left-handed in the spacecraft frame have group velocities greater than the solar wind flow and phase velocities less than the solar wind flow velocity. Right-handed waves all have velocities more nearly perpendicular to the flow, so that there is no Doppler-shifted polarization reversal. There appear to be two distinct schools of thought on the generation of these waves at Earth: bow shock generation and in situ generation from a particle resonance.

Let us first consider possible resonance mechanisms and underlying instabilities responsible for generation of these whistlers. One possible source of these waves is the backstreaming ion populations. These ions are clearly responsible for right-handed waves in the plasma frame at lower frequencies below the proton gyrofrequency [Hoppe et al., 1981; Gary et al., 1981; Russell et al., 1987]. Possible mechanisms for generating 1-Hz waves from ion beams have been discussed by Wong and Goldstein [1987, 1988] and

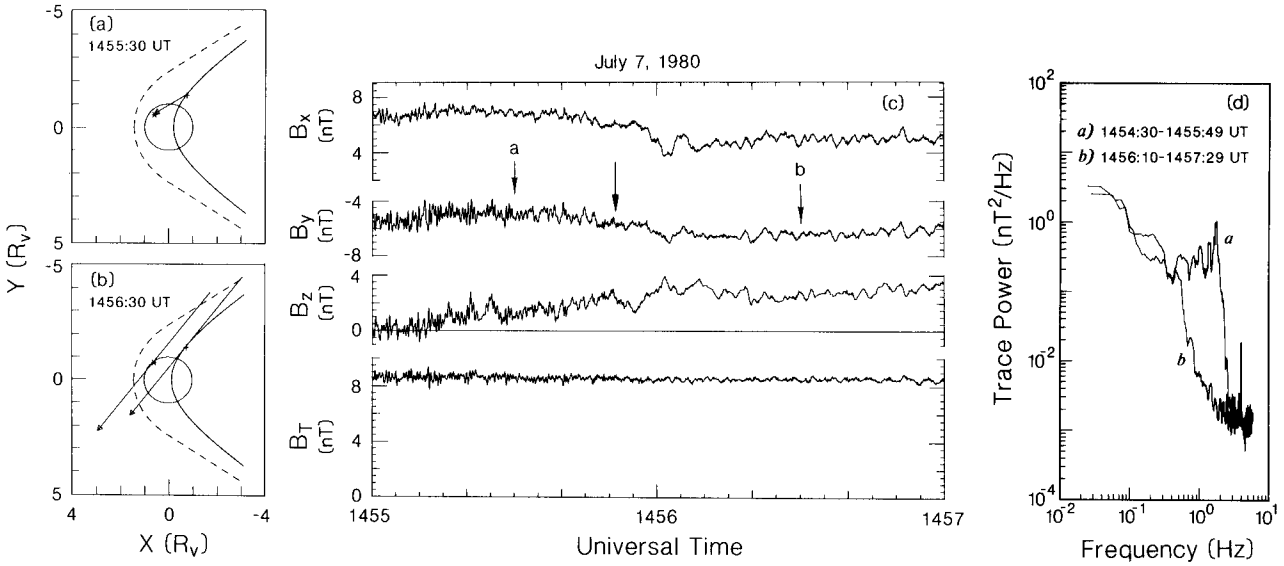

Fig. 14. (a and b) Spacecraft shock-relative position projected on the IMF-V_{sw} plane before and after disconnection. (c) Time series of the three components of the magnetic field. The IMF-Shock disconnection event is indicated by the unlabeled arrow. (d) Power spectra taken before and after the disconnection event indicating the disappearance of the wave when the IMF through the spacecraft is no longer connected to the bow shock.

Smith et al. [1989]. While we do not have a sensitive detector of upstream ions on the Pioneer Venus spacecraft, we note that our waves are extremely similar to those at Earth and therefore should have the same source. The lack of correlation of the terrestrial 1-Hz waves with any property of these ion beams thus rules out ion generation.

A second candidate for the generation mechanism for obliquely propagating waves could be the electron gyroresonance. However, there are two major problems related to this resonance. The first difficulty is that the waves generated by the electron cyclotron instability propagate obliquely and antiparallel to the direction of the electrons which stream along the magnetic field. Since as we have shown, the 1-Hz waves propagate upstream, they would be expected to be associated with downstreaming electrons as was pointed out by Russell et al. [1971]. Such a hypothesis has theoretical and observational difficulties. First, one would need a source of electrons streaming toward the shock. Second, a distribution function with $T_{perp} > T_{par}$ is needed. Neither such characteristic would be expected for upstream electrons. Moreover, as was found by Feldman et al. [1983], consistent with our results, there is a correlation between IMF-shock connection events, and the appearance of 1-Hz waves is correlated with the appearance of electrons from the shock. An additional argument against electron gyroresonance generation of the waves is that for the normal electron cyclotron instability the resonant energy of the electrons is of the order of 1 keV or greater, which is much more than the energy of the bulk of the electrons in the solar wind [see Sentman et al., 1983; Feldman et al., 1983]. Since none of the above instabilities seems to be consistent with the properties of the observed waves, we examine another instability that has been proposed by Sentman et al. [1983] to explain 1-Hz waves in the Earth's electron foreshock. It is called the oblique whistler instability, with its free energy related to the positive slope of the electron distribution function in the parallel direction, at large electron pitch angles and at energies from 20 to 50 eV. Such distribution functions have been observed upstream of the earth's bow shock by Feldman et al., [1983]. This specific electron distribution function is found when 1-Hz waves are seen on magnetic field lines connected to the bow shock [Feldman et al., 1983]. While these authors proposed that the feature in the electron distribution was due to the inhibition of reflection at lowest energies by the cross-shock potential, this proposal seems inconsistent with the observed distribution. The feature appears to be a notch in the preexisting solar wind electron distribution, and the feature does not extend to lowest energies.

Applying the linear Vlasov stability analysis of Kennel and Wong [1967] and modeling with a bi-Maxwellian, slightly anisotropic distribution function similar to that observed at the Earth, Sentman et al. [1983] found that for the actual foreshock parameters the maximum growth of the oblique whistler instability is close to θ_{kB} of 53° at a wave number, k, of 0.076 km^{-1}. Such obliquely propagating waves can grow by means of the Landau resonance in a region of positive slope in the parallel direction, lying at a very large pitch angle, 85°, with energies less than approximately 20 eV. We have no way of verifying observationally whether such electron distributions are present at Venus.

Although this latter explanation appears to be the currently accepted paradigm for the 1-Hz waves at Earth, we have several difficulties with this model. First, the model does not explain the source of the unstable electron distribution. Second, it does not explain the appearance of

right-handed waves with the same amplitude when the field line is at right angles to the flow. Instead we propose that these waves may originate in the shock as first suggested by Fairfield [1974]. The waves we see at Venus are similar in every respect to those studied by Fairfield [1974]. As shown by Tokar et al. [1984], whistler mode waves propagating upstream in the shock transition region are generated as a result of the normal electron cyclotron instability. Detailed ray tracing performed for such whistlers generated in the shock transition region [Tokar and Gurnett, 1985] indicates that if the solar wind electron distribution function is only weakly or marginally stable to the whistler mode generation, the waves will escape upstream into the foreshock. Analysis of the directions and magnitudes of the wave group velocities given in Table 3 indicates that these wave packets all could have originated at the shock. If so, as they damp, they could alter the electron distribution function, causing a notch at the resonant electron velocity, and possibly explain the origin of the "notched" electron distributions seen at Earth by Feldman et al. [1983]. This damping is consistent with the falloff in amplitude of the waves with distance from the shock shown in Figure 8 of this paper and also in Figure 4 of Orlowski et al. [1990] for Mercury, Venus, and the Earth. If the waves were growing in the foreshock, they would not have this simple relation between amplitude and shock distance. Finally, when the interplanetary magnetic field was at a large angle to the flow, as it was on July 3, 1980, shown in Figure 3, the shock would still produce these waves, but they would not be Doppler-shifted by the flow. Thus, we believe a shock source better explains the totality of observations both at the Earth and at Venus.

Conclusions

If we assume in situ generation within the foreshock, the oblique whistler instability is a potential candidate for the generation of the whistler waves similar to those observed at Venus. However, we cannot verify experimentally if there is any free energy available from large pitch angle electrons creating efficient Landau resonance with the oblique whistlers in the Venus foreshock. Moreover, we know of no mechanism for producing the necessary anisotropies in the distribution function. An attractive alternative explanation is that the waves originate in the bow shock and propagate upstream against the solar wind flow. The observed wave damping by the exchange of energy with resonant electrons could cause the notches in the electron distribution function observed in the Earth's electron foreshock and the observed decay of the wave amplitude with distance from the shock. This mechanism would also explain the appearance of right-hand polarized waves with similar amplitudes.

Acknowledgments. This work was supported by National Aeronautics and Space Administration under research grant NAG2-501.

The Editor thanks C. W. Smith and another referee for their assistance in evaluating this paper.

References

Born, M., and E. Wolf, Principles of Optics, Pergamon, New York, 1959.

Crawford, G. K., R. J. Strangeway, and C. T. Russell, Plasma waves observed in the Venus electron and ion foreshock regions, Geophys. Res. Lett., 17, 1805-1808, 1990.

Fairfield, D. H., Bow shock associated waves observed in the far upstream inter-planetary medium, J. Geophys. Res., 74, 3541-3553, 1969.

Fairfield, D. H., Whistler waves observed upstream from collisionless shocks, J. Geophys. Res., 79, 1368-1378, 1974.

Feldman, W. C., et al., Electron velocity distribution near the Earth's bow shock, J. Geophys. Res., 88, 96-110, 1983.

Gary, S. P., Microinstabilities upstream of the Earth's bow shock: Brief review, J. Geophys. Res., 86, 4331-4336, 1981.

Gary, S. P., J. T. Gosling, and D. W. Forslund, The electromagnetic ion beam instability upstream of the Earth's bow shock, J. Geophys. Res., 86, 6691-6696, 1981.

Greenstadt, E. W., and L. W. Baum, Earth's compressional foreshock boundary revisited: Observations by the ISEE 1 magnetometer, J. Geophys. Res., 91, 9001-9006, 1986.

Greenstadt, E. W., et al., Correlated magnetic field and plasma observations of the Earth's bow shock, J. Geophys. Res., 73, 51-60, 1968.

Greenstadt, E. W., et al., Whistler mode propagation in the solar wind near the bow shock, J. Geophys. Res., 86, 4511-4516, 1981.

Greenstadt, E. W., L. W. Baum, K. F. Jordan, and C. T. Russell, The compressional ULF foreshock boundary of Venus: Observations by PVO magnetometer, J. Geophys. Res., 92, 3380-3384, 1987.

Gurnett, D. A., Plasma waves and instabilities, in Collisionless Shocks in the Heliosphere: Reviews of Current Research, Geophys. Monogr. Ser., vol. 35, edited by B. T. Tsurutani and R. G. Stone, pp. 207-229, AGU, Washington, D. C., 1985.

Holzer, R. E., T. G. Northrop, J. V. Olson, and C. T. Russell, Study of waves in the Earth's bow shock, J. Geophys. Res., 77, 2269-2273, 1972.

Hoppe, M. M., and C. T. Russell, Whistler mode wave packets in the Earth's foreshock, Nature, 187, 417-420, 1980.

Hoppe, M. M., C. T. Russell, L. A. Frank, T. E. Eastman, and E. W. Greenstadt, Upstream hydromagnetic waves and their association with backstreaming ion population: ISEE 1 and 2 observations, J. Geophys. Res., 86, 4471-4492, 1981.

Hoppe, M. M., C. T. Russell, T. E. Eastman, and L. A. Frank, Characteristics of the ULF waves associated with upstream ion beams, J. Geophys. Res., 87, 643-650, 1982.

Intriligator, D. S., J. H. Wolfe, and J. D. Mihalov, The Pioneer Venus Orbiter plasma analyzer experiment, IEEE Trans. Geosci. Remote Sens., GE-18, 39-43, 1980.

Kennel, C. F., and H. V. Wong, Resonant particle instabilities in a uniform magnetic field, J. Plasma Phys., 1, 75, 1967.

Means, J., Use of the three-dimensional covariance matrix in analyzing the polarization properties

of plane waves, J. Geophys. Res., 77, 5551-5559, 1972.
Orlowski, D. S., G. K. Crawford, and C. T. Russell, Upstream waves at Mercury, Venus and Earth, Geophys. Res. Lett., 17, 2293-2296, 1990.
Russell, C. T., Planetary bow shocks, in Collisionless Shocks in the Heliosphere: Current Research, Geophys. Monogr. Ser., vol. 35, edited by E. T. Tsurutani and R. G. Stone, AGU Monograph 35, p109-130, 1985.
Russell, C. T., and M. M. Hoppe, Upstream waves and particles, Space Sci. Rev., 34, 155-172, 1983.
Russell, C. T., D. D. Childers, and P. J. Coleman, OGO 5 observations of upstream waves in the interplanetary medium: Discrete wave packets, J. Geophys. Res., 76, 845-861, 1971.
Russell, C. T., R. C. Snare, J. D. Means and R. C. Elphic, Pioneer Venus Orbiter fluxgate magnetometer, IEEE Trans. Geoscience and Remote Sens., GE-18, 32-35, 1980.
Russell, C. T., et al., Upstream waves simultaneously observed by ISEE and UKS, J. Geophys. Res., 92, 7354-7362, 1987.
Sentman, D. D., J. P. Edmiston, and L. A. Frank, Instabilities of low frequency propagating electromagnetic waves in the Earth's foreshock region, J. Geophys. Res., 86, 7487-7497, 1981.
Sentman, D. D., M. F. Thomsen, S. P. Gary, W. C. Feldman, and M. M. Hoppe, The oblique whistler instability in the Earth's foreshock, J. Geophys. Res., 88, 2048-2056, 1983.
Smith, C. W., M. L. Goldstein, and H. K. Wong, Whistler wave bursts upstream of the Uranian bow shock, J. Geophys. Res., 94, 17,035-17,048, 1989.
Sonnerup, B. U. O., Acceleration of particles reflected at a shock front, J. Geophys. Res., 74, 1301-1304, 1969.
Stix, T. H., The Theory of Plasma Waves, McGraw-Hill, New York, 1962.
Tokar, R. L., and D. A. Gurnett, The propagation and growth of whistler mode waves generated by electron beams in the Earth's bow shock, J. Geophys. Res., 90, 105-114, 1985.
Tokar, R. L., D. A. Gurnett, and W. C. Feldman, Whistler mode turbulence generated by electron beams in Earth's bow shock, J. Geophys. Res., 89, 105-114, 1984.
Wong, H. K., and M. L. Goldstein, Proton beam generation of whistler waves in the Earth's foreshock, J. Geophys. Res., 92, 12,419-12,424, 1987.
Wong, H. K., and M. L. Goldstein, Proton beam generation of oblique whistler mode waves, J. Geophys. Res., 93, 4110-4114, 1988.

D. S. Orlowski and C. T. Russell, UCLA, IGPP, 405 Hilgard Avenue, Los Angeles, CA, 90024

(Received December 26, 1990;
revised March 18, 1991;
accepted April 11, 1991.)